university of groningen

University Medical Center Groningen

University of Groningen

Probing the mass distribution in groups of galaxies using gravitational lensing

Möller, Ole; Natarajan, P.; Kneib, J. P.; Blain, A. W.

Published in:
The Astrophysical Journal

DOI:
10.1086/340655

IMPORTANT NOTE: You are advised to consult the publisher's version (publisher's PDF) if you wish to cite from it. Please check the document version below.

Document Version
Publisher's PDF, also known as Version of record

Publication date:
2001

Link to publication in University of Groningen/UMCG research database

Citation for published version (APA):
Möller, O., Natarajan, P., Kneib, J. P., & Blain, A. W. (2001). Probing the mass distribution in groups of galaxies using gravitational lensing. *The Astrophysical Journal*, *573*(2), 562-575. https://doi.org/10.1086/340655

Copyright
Other than for strictly personal use, it is not permitted to download or to forward/distribute the text or part of it without the consent of the author(s) and/or copyright holder(s), unless the work is under an open content license (like Creative Commons).

The publication may also be distributed here under the terms of Article 25fa of the Dutch Copyright Act, indicated by the "Taverne" license. More information can be found on the University of Groningen website: https://www.rug.nl/library/open-access/self-archiving-pure/taverne-amendment.

Take-down policy
If you believe that this document breaches copyright please contact us providing details, and we will remove access to the work immediately and investigate your claim.

Downloaded from the University of Groningen/UMCG research database (Pure): http://www.rug.nl/research/portal. For technical reasons the number of authors shown on this cover page is limited to 10 maximum.

Download date: 05-05-2023

The Astrophysical Journal, 573:562–575, 2002 July 10
© 2002. The American Astronomical Society. All rights reserved. Printed in U.S.A.

PROBING THE MASS DISTRIBUTION IN GROUPS OF GALAXIES USING GRAVITATIONAL LENSING

Ole Möller,[1,2] Priyamvada Natarajan,[3] Jean-Paul Kneib,[4] and A. W. Blain[5,6]
Received 2001 September 25; accepted 2002 March 12

ABSTRACT

In this paper, we present a numerical study of gravitational lensing by groups of galaxies. Since groups are abundant and therefore have a large covering fraction on the sky, lensing by groups is likely to be very important observationally. Besides, it has recently become clear that many models for strong lensing by individual galaxies require external shear to reproduce the observed image geometries; in many cases a nearby group is detected that could provide this shear. In this work, we study the expected lensing behavior of moderate-redshift analogs of compact galaxy groups in both the weak- and strong-lensing regimes. We show how measurements of the tangential shear can be used to determine whether groups possess a massive common group halo or whether most of the mass is associated with the individual galaxies. From our simulations, we find that the peak value of the weak-lensing shear signal is of the order of 3% and varies by a factor of about 2 for different assumed mass distributions. We demonstrate that these variations are large enough to be detectable with 3 σ confidence from space with the Advanced Camera for Surveys on the *Hubble Space Telescope* with only 100 groups, or alternatively with 2 σ confidence from the ground with about 200 groups, by stacking high-quality images. In the strong-lensing regime, we find that the image geometries and typical magnifications are sensitive to the group properties and that groups can easily provide enough external shear to produce quadruple images. We investigate the statistical properties of lensing galaxies that are near to or part of a group and find that properties such as the distribution of time delays are affected measurably by the presence of the group, which can therefore introduce an additional systematic error in the measurement of the Hubble constant from such systems. We conclude that both the detection of weak lensing by groups and accurate observations of strong galaxy lens systems near groups could provide important information on the total mass and matter distribution within galaxy groups.

Subject headings: dark matter — galaxies: clusters: general — gravitational lensing

1. INTRODUCTION

Within the context of the current paradigm for structure formation—gravitational instability in a cold dark matter–dominated universe leading to mass hierarchies—clusters and isolated galaxies are at extreme ends of the mass spectrum of collapsed structures. Clusters, the most massive virialized objects, have the highest density contrast and are rare, whereas galaxies are less massive and more abundant. In this scenario, groups of galaxies, which lie in the intermediate-mass range between galaxy clusters and individual galaxies, are the most common gravitationally bound entities at the present epoch (Ramella, Pisani, & Geller 1997). Galaxy groups contain between three and 30 galaxies, and they trace the large-scale structure of the universe (Ramella et al. 1999). The abundance of compact groups was estimated by Barton et al. (1996) to be quite high, $1.4 \times 10^{-4}\ h^3$ Mpc^{-3}. It is likely that they contribute significantly to the mass density of the universe, Ω_M. However, little is known about the detailed mass distribution in groups of galaxies; probing the mass of groups and the mass distribution within groups is likely to be crucial to understanding the evolution of both dark and baryonic matter.

Gravitational lensing provides a very useful tool to determine the mass distribution in structures on a range of scales, and in this paper we demonstrate how weak and strong lensing may be used to determine the mass distribution within groups of galaxies.

In the past, gravitational lensing by isolated galaxies and clusters of galaxies has been used extensively both as a cosmological tool (Bartelmann et al. 1998; Wambsganss, Cen, & Ostriker 1998) and as a method to map detailed mass distributions (Mellier 1999). In the weak-lensing regime, reconstruction methods have provided moderate-resolution shear maps (Hoekstra et al. 1998; Clowe et al. 2000; Hoekstra, Franx, & Kuijken 2000). In analyses that combine both weak- and strong-lensing data for clusters it is found that further constraints can be obtained on the clumpiness of the dark matter distributions on smaller scales within clusters (Natarajan & Kneib 1997; Geiger & Schneider 1999).

In this paper, we investigate the strong- and weak-lensing properties of groups of galaxies using numerical ray-tracing simulations. We show in particular how it is possible to determine whether the mass within groups resides in a common halo or whether it is associated with the individual galaxies using weak- and/or strong-lensing observations.

In § 2 a brief overview of galaxy groups is presented, concentrating on the properties of the observed compact Hickson groups (Hickson 1982; Hickson et al. 1988), followed by a description of the properties of the simulated groups. In § 3 the lensing properties of the mass models is outlined along with a brief description of the numerical analysis techniques. Section 4 focuses on the expected weak-lensing signal from groups of galaxies, its dependence on group properties, and the feasibility for detection. In § 5 the effects

[1] Cavendish Laboratory, Madingley Road, Cambridge, CB3 OHE, UK.
[2] Kapteyn Institute, P.O. Box 800, 9700 AV Groningen, Netherlands.
[3] Department of Astronomy, Yale University, 265 Whitney Avenue, New Haven, CT 06511.
[4] Observatoire Midi-Pyrénées, UMR5572, 14 Avenue Edouard Belin, F-31400 Toulouse, France.
[5] Institute of Astronomy, Madingley Road, Cambridge CB3 0HA, UK.
[6] Department of Astronomy, California Institute of Technology 105-24, Pasadena, CA 91125.

of a group in the vicinity of a strong galaxy lens are studied. The paper concludes with a summary of the results and suggestions for a possible strategy for constraining the detailed mass distribution within galaxy groups in § 6.

2. PROPERTIES OF GALAXY GROUPS

Detected galaxy groups have been found in two primary configurations: compact and loose. Compact groups have been cataloged by Hickson (1982) and are easily identified on the sky because of the high projected overdensity of member galaxies, but they might not be truly representative of groups as a whole. There has been some recent evidence from the studies of a large sample of loose groups (Helsdon & Ponman 2000) that the correlations observed between their properties, such as X-ray luminosity, velocity dispersion, and temperature, differ from those of compact groups studied by Mulchaey & Zabludoff (1998). The mass function of nearby galaxy clusters follows a Press-Schechter (1974) form, and recent studies have shown that the mass function of loose groups follows a similar distribution (Girardi & Giuricin 2000), suggesting a continuity of clustering properties from groups to rich clusters. However, the detailed mass distribution *within* galaxy groups has not been investigated so far. In particular, it is still not totally clear whether the majority of groups possess a massive group dark matter halo. X-ray surface brightness profiles seem to point toward the existence of a common group halo for compact groups (Ponman et al. 1995; Helsdon et al. 2001), as extended and diffuse X-ray emission is detected from the group as a whole, although it is often observed to be centered around the optically brightest galaxy in the group (Mahdavi et al. 2000). Also, some recent work suggests that poor groups of galaxies can be identified unambiguously as bound structures only if they are X-ray luminous and that most of the mass in these groups is associated with a common group halo that is not necessarily centered on the brightest member (Zabludoff & Mulchaey 1998). Therefore, the observational evidence at the present time regarding the mass distribution in nearby groups points to the existence of a large-scale group halo.

The precise morphology of the dark matter distribution in groups can provide important theoretical constraints on their formation and future evolution. Gravitational lensing offers an elegant method to map the mass content of the group and a first observational detection of weak lensing by groups has been reported by Hoekstra et al. (2001). For 50 groups selected from the Canadian Network for Observational Cosmology Galaxy Redshift Survey (CNOC2) at $z = 0.12$–0.55, a typical mass-to-light ratio in solar units in the B band of $191 \pm 83\,h$ is reported, indicating the presence of significant amounts of dark matter in groups. Since the lensing effects of individual galaxies are detectable at a significant level (commonly referred to as galaxy-galaxy lensing; see Brainerd, Blandford, & Smail 1996; Fischer et al. 2000; Hudson et al. 1998; dell'Antonio & Tyson 1998; McKay et al. 2001; Wilson et al. 2001), we expect an unambiguous signal to be obtained for groups.

In this work, we discuss the lensing properties of compact groups of galaxies in the weak- and strong-lensing regime in more detail using numerical ray-tracing techniques. Our choice to concentrate on compact groups is motivated mainly by the fact that they can be easily identified. In general, the identification of groups and the establishment of membership has proven to be observationally difficult because of the ambiguity arising from chance superpositions on the sky (Hickson et al. 1992; de Carvalho & Djorgovski 1995; Barton et al. 1996; Zabludoff & Mulchaey 1998, 2000).

2.1. *Analytic Forms for the Potential*

The fiducial model studied here is a four-member compact group—a moderate-redshift analog of the nearby Hickson groups. The total projected surface mass density at position $\boldsymbol{r}$ is simply the sum of the surface mass densities of the individual galaxies, Σ_i, plus a larger scale smooth component Σ_h, that defines a larger scale group halo encompassing all the individual galaxies:

$$\Sigma(\boldsymbol{r}) = \Sigma_h(\boldsymbol{r}) + \sum_{i=1}^{4} \Sigma_i(\boldsymbol{r} - \boldsymbol{r}_1) \; . \tag{1}$$

Individual galaxies and the larger scale group halo are modeled as scaled, self-similar pseudoisothermal elliptical mass distributions (PIEMDs; Kassiola & Kovner 1993), parameterized by ellipticity ϵ, scale length r_s, truncation radius r_t, and central density ρ_0. The projected surface density for such a model is

$$\Sigma_i(\boldsymbol{r}) = \Sigma_0 \frac{r_s r_t}{r_t - r_s} \left[\frac{1}{\sqrt{r_0^2 + k^2(x,y)}} - \frac{1}{\sqrt{r_c^2 + k^2(x,y)}} \right] , \tag{2}$$

where

$$k(x,y) = \sqrt{x^2/(1+\epsilon)^2 + y^2/(1-\epsilon)^2} \; .$$

In the limit of a spherical halo, $\epsilon = 0$, the projected mass enclosed within radius R is simply

$$M(R) = \frac{M_{\rm tot}}{(r_t - r_s) R c^2} \left[\sqrt{r_s^2 + r^2} - \sqrt{r_t^2 + r^2} + (r_t - r_s) \right] , \tag{3}$$

where $M_{\rm tot} = 2\pi\Sigma_0 r_s r_t$ is the total mass, which is finite.

These self-similar PIEMDs provide a reasonable, realistic model of the mass distribution in the both the large-scale smooth component as well as the mass associated with early-type galaxies and have been used previously successfully to model the mass profile of individual galaxies in clusters by Natarajan & Kneib (1997; Natarajan et al.1998).

2.2. *Properties of Simulated Groups*

Each simulated group is defined by its redshift, z_l; the masses of the constituent galaxies, M_i; their positions, $\boldsymbol{r}_1$, scale lengths, r_g; ellipticities, ϵ_i; and inclination angle measured with respect to the x-axis, ϕ_i. The group halo is assumed to be a spherical, pseudoisothermal component with mass M_h centered on the mass weighted mean position of the individual galaxies. Real halos are likely to be elliptical in general (as opposed to spherical), but since we focus here on the average lensing signal of a large sample of groups, this simplifying assumption will not have a significant effect on our results. Most defining parameters that characterize the group properties are determined by drawing randomly from probability distributions using a standard algorithm described in Press et al. (1988). Characteristic values for the parameters for the simulated groups are tabulated below.

2.2.1. *Group Redshift*

The simulated groups were chosen to lie at a redshift of $z_l = 0.3$, which corresponds approximately to the most effective lens redshift for background sources with a mean redshift of $z \sim 1$. Owing to the difficulty of detecting and identifying groups, most known compact groups are at a redshift substantially less than $z = 0.3$, and as mentioned previously, we are concentrating here on the higher redshift analog of currently detected groups at low redshift. However, new surveys, such as the Sloan Digital Sky Survey, should provide a large number of candidate groups at redshifts of order 0.3 which can then be fruitfully followed up with observations using the Advanced Camera for Surveys (ACS) that is to be installed on the *Hubble Space Telescope* (*HST*) shortly. In § 4.3 we show qualitatively how variations in the redshift of the group and possible projection effects due to the effect of two groups lying at different redshifts along the same line of sight affect our results. Note that for the cosmological model of choice, $H_0 = 50\ h_{50}$ km s^{-1} Mpc^{-1}, $\Omega_M = 0.3$, and $\Omega_\Lambda = 0.7$, an angular separation a $1''$ corresponds to 6.24 kpc at a redshift of $z = 0.3$.

2.2.2. *Galaxy Positions*

The individual galaxy positions within each group are randomly generated using a number density profile,

$$N(\boldsymbol{r}) = \frac{N_0}{\left(1 + r^2/r_N^2\right)^\beta}\ , \tag{4}$$

where r_N is the assumed typical group scale length. We use a value of $\beta = 3/2$, which corresponds to the modified Hubble-Reynolds law everywhere in this paper except in § 4.2. The normalization N_0 is determined by requiring

$$\int_0^\infty N(\boldsymbol{r}) d^2\boldsymbol{r} = N_{\rm gal}\ . \tag{5}$$

In § 4.2 the effects of the choice of the distribution of the galaxy scale lengths and the form of the number density profile on the results are discussed further.

2.2.3. *Galaxy Mass Profiles*

Group members are modeled by a PIEMD, given in equation (2). A suitable set of parameters for this profile are scale length r_g, total mass M_g enclosed within a radius $R = 100$ kpc, and an ellipticity ϵ. Figure 1 shows the average enclosed surface mass density as a function of radius for various choices of scale length and mass compared to the point mass case.

Note that for small core radii the results do not depend strongly on the choice of r_s. To generate parameters for the galaxies, we determine the scale lengths randomly from a Gaussian distribution of mean $\widetilde{r_g}$ and width σ_{rg},

$$P_{rg}(r_g) = \frac{1}{\sqrt{2\pi}\sigma_{rg}} \exp\left[-\frac{(r_g - \widetilde{r_g})^2}{2\sigma_{rg}}\right]\ . \tag{6}$$

with the additional physical requirement that $0 < r_g$. The average scale length is $\langle r_g \rangle \approx \sigma_{rg}/\sqrt{2}$. In a similar fashion, we draw the ellipticities from a Gaussian distribution with a mean of zero and a standard deviation $\sigma_\epsilon = 0.3$ with the requirement that $\epsilon > 0$ so that the average $\langle \epsilon \rangle = 0.2$. The mass M_g is similarly determined randomly from a Gaussian distribution, with $0 < M_g$ so that the average mass $\langle M_g \rangle \approx 1/\sqrt{2}\sigma_M$. The distribution of the orientation angle of the galaxies with respect to the x-axis, ϕ_i is assumed to be uniform.

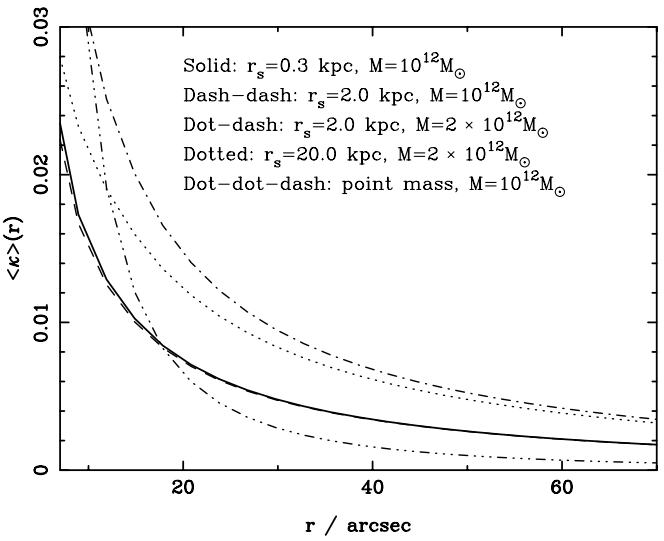

FIG. 1.—Average surface mass density enclosed inside a circle of radius r for the mass profile given by eq. (2), compared to that of a point mass. The mass M labeling the various style types is the total mass contained within a radius of 100 kpc. Note that $\kappa \ll 1$ in all cases.

2.2.4. *Group Halo*

The primary motivation for this study is to investigate the possibility of determining the fractional mass of any common intergalactic group halo that might be present in compact groups. These larger scale smooth group halos are also modeled using a PIEMD of the same form as that for the member galaxies, (i.e., eq. [2]), centered on the mean geometrical position of all galaxies. The parameters describing the intergalactic halo are therefore also scale length, r_h and total mass, M_h within a cutoff radius R. The halo scale length is determined from a Gaussian distribution in the same way as is done for the galaxies scaled appropriately. The corresponding statistical mean mass and standard deviation, $\widetilde{r_h}$ and σ_{rh}, are, respectively, listed in Table 1. The halo mass is determined by the masses of the individual galaxies,

$$M_h = f \times M_{\rm tot} = \frac{f}{1-f} \sum_{i=0}^{4} M_i\ , \tag{7}$$

where $M_{\rm tot}$ is the total mass in the group and f denotes the total mass fraction in the halo, $0 < f < 1$. Observationally, we are likely to have a better handle on the masses of the individual galaxies than on the total mass of the group. We can then estimate the total mass of the group if we can obtain a value for f; this can in fact be done with weak lensing as is described below in § 4. Alternatively, if the total group mass is determined from other techniques such as X-ray observations, then strong lensing could be used to constrain the mass of constituent members; this approach is described in § 5.

3. LENSING PROPERTIES OF GROUPS

The total surface mass density Σ induces a convergence κ and shear γ in the shapes of the background source popula-

TABLE 1
List of the Parameters Used in This Paper

Parameter	Symbol	Value[a]
Hubble parameter	h	0.5
Matter density	Ω_M	0.3
Cosmological constant	Ω_Λ	0.7
Lens redshift	z_l	0.3
Source redshift	z_s	1.0
Number of group members	$N_{\rm gal}$	4
Group scale length (kpc)	r_N	15–40
Gaussian mean galaxy scale length (kpc)	$\widetilde{r_g}$	0.2
Variance of galaxy scale length (kpc)	σ_{rg}	0.07
Variance of galaxy ellipticities	σ_ϵ	0.3
Mean galaxy mass ($M_\odot$)	$\widetilde{M_g}$	10^{12}
Variance of galaxy mass ($M_\odot$)	σ_M	5×10^{11}
Gaussian mean halo scale length (kpc)	$\widetilde{r_h}$	15
Variance in halo scale length (kpc)	σ_{rh}	3
Cut off radius for the group halo (kpc)	R	100
Fraction of total mass in halo	f	0–1

Note.—Both cosmological parameters and parameters that define the group properties are listed.
[a] Unless otherwise stated.

tion located on a sheet at redshift z_s. We obtain dimensionless forms for the surface mass density, potential, and shear in the usual way by defining the convergence $\kappa(\boldsymbol{r}) = \Sigma(\boldsymbol{r})/\Sigma_c$, scaled in units of the critical surface mass density $\Sigma_c = c^2 D_S/4\pi G D_L D_{LS}$, where D_{OS}, D_{OL} and D_{LS} are the angular diameter distances from observer to source, from observer to lens and from lens to source, respectively, as evaluated in a smooth FRW universe. The dimensionless form of the gravitational potential can then be written as

$$\psi(\boldsymbol{r}) = \frac{1}{\pi}\int \kappa(\boldsymbol{r}) \ln(|\boldsymbol{r} - \boldsymbol{r}|) d^2 r' \ . \quad (8)$$

For a pseudoisothermal sphere this potential can be written analytically as

$$\psi(\boldsymbol{r}) = \frac{\Sigma_0 r_0 r_c}{r_c - r_0}[X - Y - r_0 \ln(r_0 + X) + r_c \ln(r_c + Y)] \ , \quad (9)$$

where $X = \left(r_0^2 + r^2\right)^{1/2}$ and $Y = (r_c^2 + r^2)^{1/2}$. The components of the shear are given by

$$\gamma_1 = \frac{1}{2}\left(\frac{\partial^2\psi}{\partial^2 x} - \frac{\partial^2\psi}{\partial^2 y}\right) \ , \quad (10)$$

$$\gamma_2 = \frac{\partial^2\psi}{\partial x \partial y} = \frac{\partial^2\psi}{\partial y \partial x} \ , \quad (11)$$

and the magnification μ is given by

$$\mu = \frac{1}{(1-\kappa)^2 - \gamma^2} \ . \quad (12)$$

We are concerned here with the measured shear produced by gravitational lensing, the observable quantity is in fact the "reduced shear," which is a combination of κ and γ,

$$\boldsymbol{g} = \frac{\gamma}{1-\kappa} \ , \quad (13)$$

and is directly related to the induced ellipticity of a circular background source (Bartelmann & Schneider 2001). It is useful to quantify the tangential shear in terms of the components γ_1 and γ_2; for example, to define an aperture mass (Kaiser 1995; Schneider et al. 1998),

$$\gamma_T = \gamma_1 \sin 2\phi + \gamma_2 \cos 2\phi \ , \quad (14)$$

where ϕ is the angle between $\boldsymbol{\gamma}$ and the x-axis of the coordinate system.

Since our results are obtained using numerical simulations, we refrain from presenting any further analytic formulae. Figure 2 shows the tangential shear produced by a spherical galaxy profile as a function of radius (which is defined as the distance from the center of mass) for a range of scale lengths and masses.

The magnitude of the shear at $r \approx 10''$, of about 2%, is consistent with the findings from galaxy-galaxy lensing as well as Hoekstra et al. (2001). Note that the effect of a large core radius r_s is to reduce the shear in the innermost regions $r < r_s$ below the value that is predicted at large distances. Large core radii are not observed in galaxies since no demagnified central image has ever been observed in a multiply-lensed QSO system, arguing in favor of a compact mass distribution (Cohn et al. 2001); however, extended group halos could in principle possess large cores.

3.1. *Numerical Methods*

The lens equation for groups is solved using the ray-tracing code described in Möller & Blain (1998, 2001). With the exception of § 4.3, we use a single lens plane, as all group members are assumed to have very similar redshifts. The deflection angle at position vector $\boldsymbol{r}$ in the lens plane is then calculated numerically from the expression of the surface mass density as given in equations (1) and (2) using the formalism for elliptical profiles developed by Schramm (1990). The adaptive grid method as described in Möller & Blain (2001) is especially suitable for the study of multiple lens systems such as groups of galaxies, as it increases the achievable resolution around regions of interest by a large factor.

3.1.1. *Weak Lensing*

In order to compute weak lensing by groups of galaxies, we generate a fine grid of $N = n_x \times n_y \sim 10^6$ pixels, which are assigned reduced shear values obtained from a numeri-

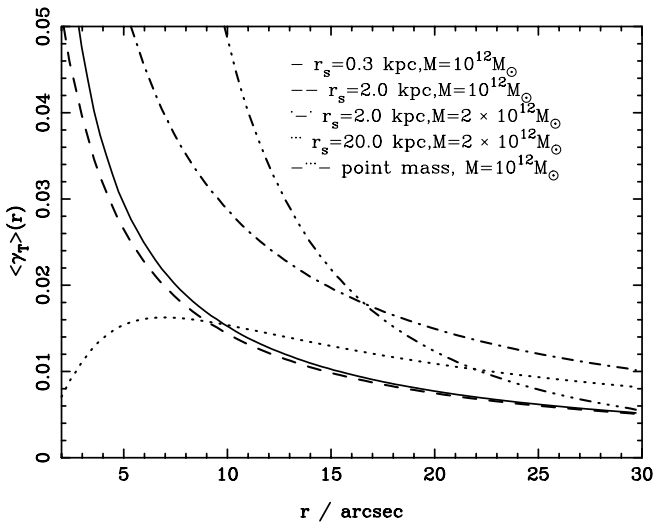

Fig. 2.—Average tangential shear at radius r for the mass profiles in Fig. 1.

cal ray-tracing simulation. From this fine grid, we determine the reduced shear profile for different group models. The numerical error in these simulations is negligible.

3.1.2. *Strong Lensing*

The magnification maps on the source and image plane are obtained using the ray tracing of triangles as described in Schneider, Ehlers, & Falco (1992) and Möller & Blain (2001). The number of images on a regular grid in the source plane are also obtained using the same ray-tracing routines. For every point on this grid, we store the number of images, the image positions, magnifications, and time delays for each individual image. This information is used to obtain the statistical properties presented in § 5.2. The time delay ΔT between two images, at $\boldsymbol{\theta}_1$ and $\boldsymbol{\theta}_2$, of a source at $\boldsymbol{\beta}$ is obtained using the equation

$$\Delta T = C \times (1 + z_l) \left[\frac{(\boldsymbol{\beta} - \boldsymbol{\theta}_1)^2 - (\boldsymbol{\beta} - \boldsymbol{\theta}_2)^2}{2} + \Delta\psi \right] . \quad (15)$$

where $C = (D_{OS} D_{OL})/(c D_{LS})$, $\Delta\psi = \psi(\boldsymbol{\theta}_2) - \psi(\boldsymbol{\theta}_1)$ and the potential ψ itself is given by equation (8).

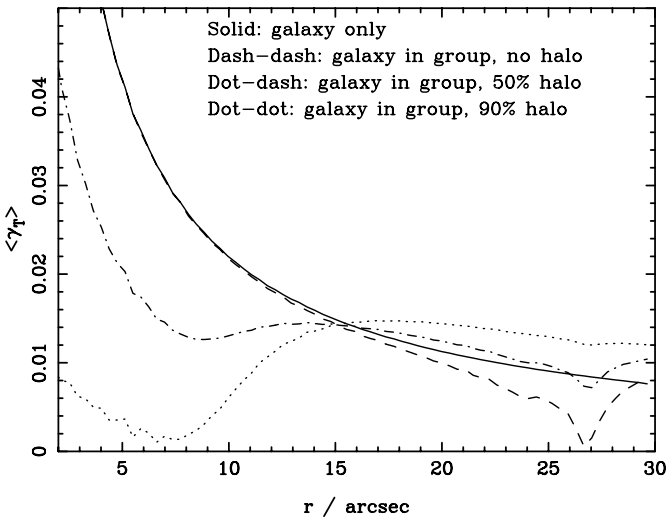

FIG. 3.—Average tangential shear computed centered at a group member, for different values of the halo-to-galaxy mass ratio. The total group mass is the same in all cases. The solid line shows the shear for an isolated galaxy for comparison.

4. WEAK LENSING BY GROUPS

Weak gravitational lensing provides an extremely useful tool to map mass distributions on large scales, ranging from a few hundred kiloparsecs to a megaparsec. The shear of background galaxies around clusters, which in the weak regime is at the 1%–10% level, has been used quite successfully to determine the cluster potential (Hoekstra et al. 1998; Fischer 1999; Clowe et al. 2000); but, because of their smaller mass, the signal from galaxy groups is expected to be lower. The mass contrast from groups is similar to or greater than that from large-scale structure, and so recent progress in sensitivity and methods has made the detection of weak-lensing signals by groups feasible (Hoekstra et al. 2001). An individual compact group occupies a small area on the sky; therefore, the essential limitation is due to the small number of background galaxies that lie directly behind the group. To detect a significant signal several groups have to be stacked, akin to the case of galaxy-galaxy lensing (Brainerd, Blandford, & Smail 1996; Fischer et al. 2000; Hudson et al. 1998; dell'Antonio & Tyson 1998; McKay et al. 2001; Wilson et al. 2001), in order to increase the signal-to-noise ratio. The distinguishable effects of the choice of different group mass profiles on the resultant averaged, stacked shear map from a sample of about 100 random groups is studied in this section.

4.1. *Distinguishing Group Halo versus Individual Halos*

In Figure 3 the effect of varying the ratio of mass in the group halo to that associated with individual group member galaxies is plotted for the detected shear signal centered around an individual member. Increasing the fraction of mass attributed to the group halo leads to a lowering of the shear signal at small radii. The reduction of the shear in the inner regions is primarily due to the relatively small mass contribution of the individual galaxies and is compensated by the increase in the external shear produced by the presence of the halo, introducing an asymmetry in the shear pattern. This is a generic effect that is found in the lensing signal of all member galaxies, but its strength varies depending on the relative positions of the galaxies and halo. In Figures 4*a*–4*d* we show shear and magnification maps for a group varying the halo to galaxy mass ratio keeping the total group mass fixed.

The shear signal within 20″varies by about 1%. There is, however, some uncertainty, as we do not have a priori knowledge of the profile slope and core radius of the intergalactic group halo. A possibility would be to use the X-ray profile and assume that the same form describes the mass distribution in the halo. Another difficulty arises from the fact that it is necessary to determine the position of the "center" of the group in order to stack the tangential shear signal coherently. If either this determination is inaccurate or the intergalactic halo is off-center from this position, then the measured shear profile will be flatter, leading to a systematic underestimate in the halo mass fraction. An elegant solution to these problems is to add the average tangential shear around each member galaxy (Fig. 5). The positions of galaxies can be determined accurately from their light distribution. Furthermore, the slope of the mass profile of the individual galaxies is much better constrained from the studies of individual lenses. Since the constraints on the positions and profiles of the individual galaxies are likely to be tighter, the average shear profile around each of the member galaxies can then be related directly to the group halo to galaxy mass ratio. Determining the shape of the average shear profile around a set of galaxies can therefore provide a new, important, and feasible way of determining the relative mass fraction in galaxies in different environments. Figure 6 shows the resulting shear profile around the member galaxies averaged over 100 groups.

Qualitatively, the same effect is seen in both cases (independent of choice of center), a strong correlation between the relative mass distributions and the average value of the shear; however, for the case of massive large-scale group halos, the average shear around group members is significantly reduced at small radii. In the following sections the average shear around the member galaxies, rather than the shear around the ill-defined group center, will be considered.

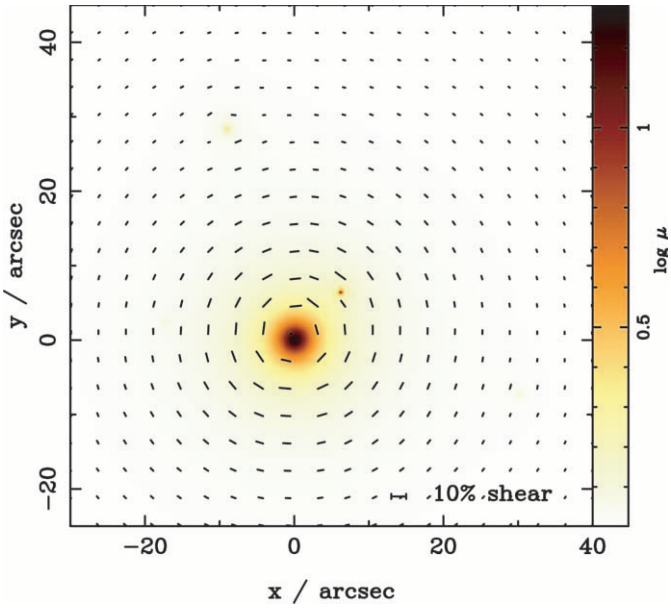

FIG. 4*a*

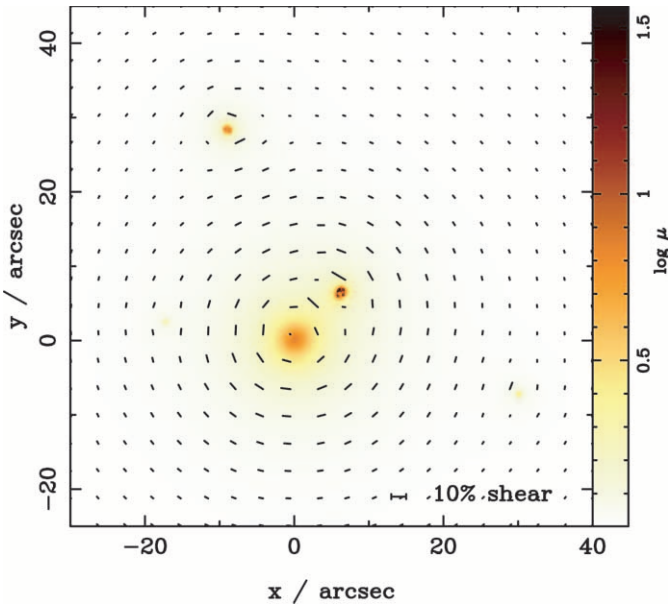

FIG. 4*b*

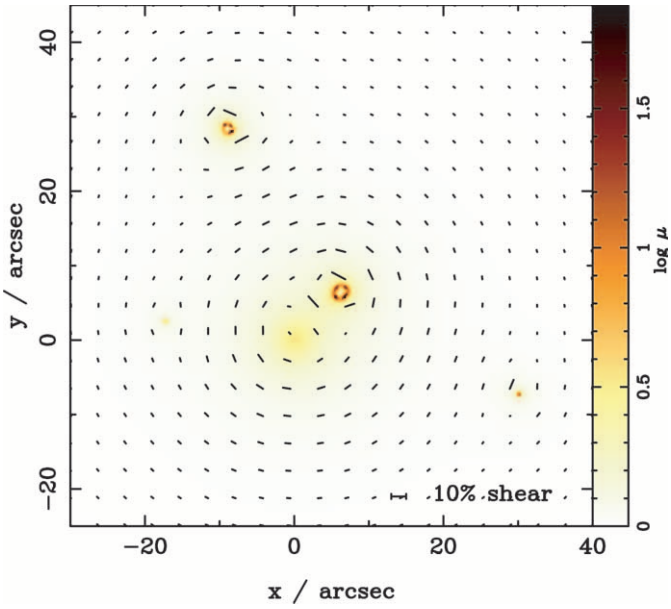

FIG. 4*c*

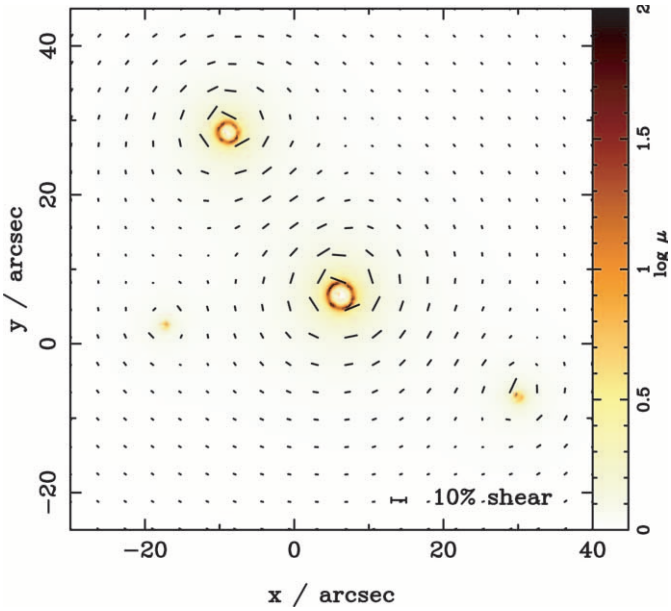

FIG. 4*d*

FIG. 4.—Shear and magnification maps for a typical compact group with four member galaxies. The panels show the magnification on the image plane as a gray scale. The direction and relative magnitude of the shear is indicated by the arrows in each panel: (*a*) is for a group corresponding to model A in table 2, (*b*) is for a group corresponding to model B, and (*c*) is for a group corresponding to model C; (*d*) shows the shear and magnification for a group as in model D, with no halo. In all panels, the source plane redshift is taken to be $z_s = 1.0$.

4.2. *Dependence on the Density Profile of Galaxies in the Group*

The galaxy profile given in equation (2) has been used extensively and provides a good approximation to the true mass profile of most galaxies. Furthermore, past studies have shown that galaxies have compact core radii, and as shown in Figure 2, the observed shear variations with galaxy core radius and ellipticity are expected to be small. The effect of the choice of the form of the galaxy number density profile on the measured shear is shown in Figure 7.

The figure shows that for number density profiles steeper than the modified Hubble-Reynolds law, the average tangential shear at radii of about 30″ is increased relative to the inner average shear. This is due to an increase in the average mass density both inside the group and around member galaxies for more spatially compact groups.

The analysis presented here mainly concerns the study of small compact groups. We also performed simulations for group scale lengths between 15 and 40 kpc and found that the shear profile does not vary significantly; this is as we expect given that we normalize the mass at a relatively small radius of 100 kpc.

Recently, there has been much discussion about the NFW (Navarro, Frenk, & White 1996) density profile, which has been fitted successfully in *N*-body simulations to

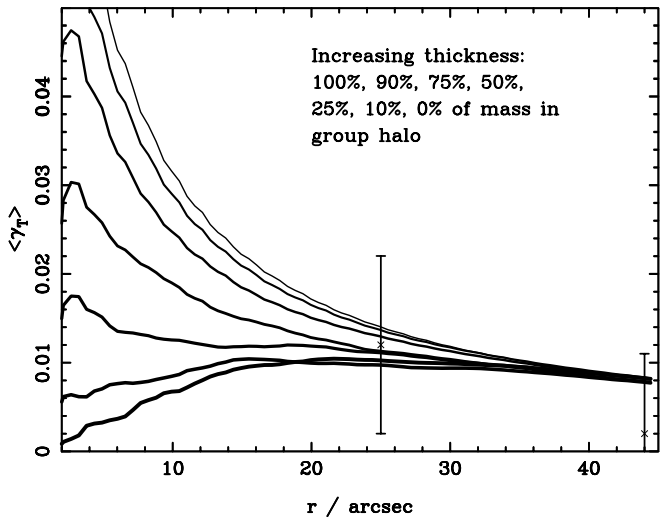

FIG. 5.—Tangential shear averaged over 100 groups for different values of the halo mass : galaxy mass ratio. Groups are stacked so that the centers of mass coincide. The total group mass is the same in all cases. The overplotted observational data point is from Hoekstra et al. (2001) for the CNOC2 groups.

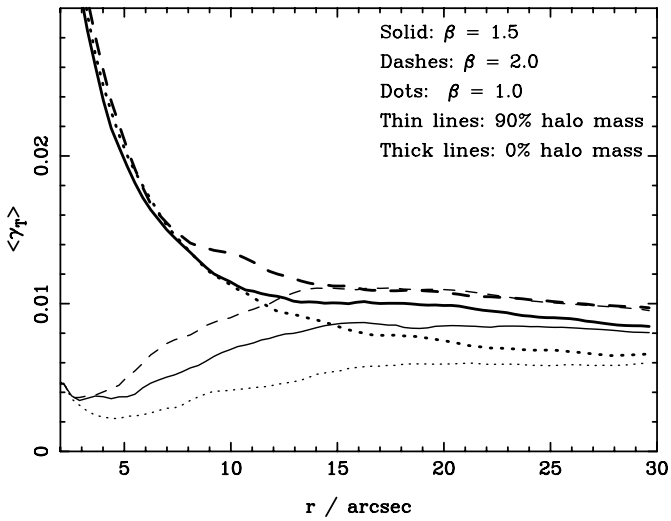

FIG. 7.—Average tangential shear around the individual group members of 100 simulated groups for different shapes of the galaxy number density profile, eq. (4). The groups are generated randomly, as described in § 2.2 and are all at $z_l = 0.3$.

dark matter halos on a large range of scales from small galaxies to rich clusters. The lensing properties of this profile have been studied recently by Wright & Brainerd (2000). We explore this density profile for group members in our simulations in order to verify that our results presented in the previous sections remain, qualitatively, the same. The NFW profile has the form

$$\rho(r) = \frac{\rho_0}{r/r_s(1 + r/r_s)^2} , \qquad (16)$$

where r_s is a characteristic scale length and ρ_0 is a central density. The total mass interior to radius R for an NFW profile is

$$M(r) = 4\pi\rho_0 r_s \left[\ln\left(1 + \frac{r}{r_s}\right) - \frac{r}{r + r_s}\right] . \qquad (17)$$

Analytical expressions for the shear can be found in Wright & Brainerd (2000) and Trentham, Möller, & Ramirez-Ruiz (2000). The scale lengths for this galaxy model are assigned randomly in exactly the same way as for the PIEMD, as described in § 2.2. The total mass inside a radius of 100 kpc is set to the same value as for the PIEMD. Since the NFW profile is shallower inside r_s and steeper outside that radius as compared with the PIEMD profile, the mass at small radii is larger than that for the equivalent PIEMD. The shear signal is therefore expected to be larger at small radii. Figure 8 shows the tangential shear around a group in which all the mass components are modeled as NFW profiles.

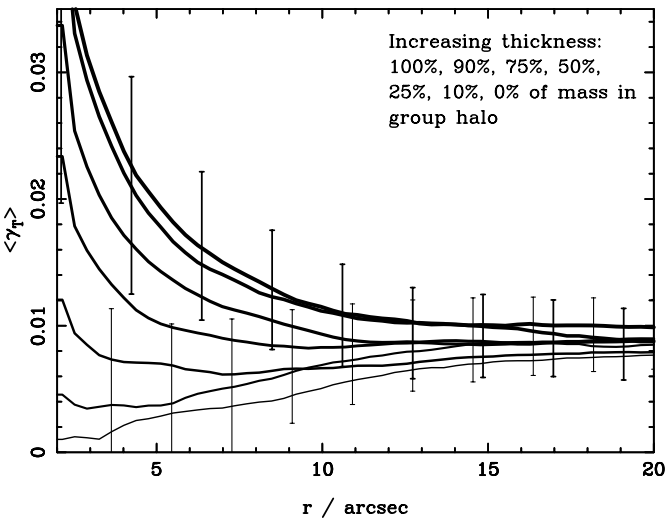

FIG. 6.—Average tangential shear around the individual group members of 100 simulated groups for different halo : galaxy mass ratios. The qualitative behavior is similar to that in Fig. 5; the signal at small radii is strongly dependent on the relative masses of galaxy and group halos. Note that the difference between this plot and the previous one lies in the choice of center around which the shear field is averaged. For the two extreme cases, the vertical bars show the 3 σ errors that would be obtained if 100 groups would be observed with the ACS, as described in § 4.4.

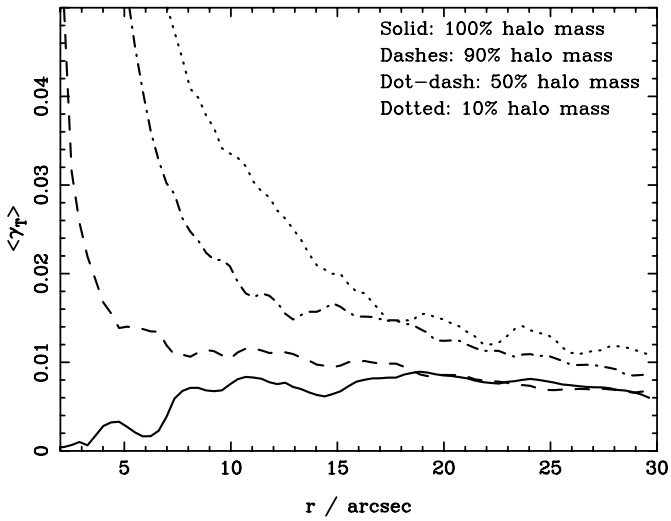

FIG. 8.—Average tangential shear around the individual group members of 100 simulated groups for an NFW galaxy and halo profile. The group properties are determined randomly as for Figs. 2–5. All groups are at $z_l = 0.3$ and the source redshift $z_s = 1.0$.

Results are qualitatively similar to those obtained for the PIEMDs (in Fig. 3). However, the effect on the shear field of shifting mass from the halo to the individual galaxies is much more pronounced owing to the larger mass contained at small radii in the NFW: the central value of the shear is even more sensitive to the halo mass to galaxy mass ratio, and the shear at small radii is generally larger.

4.3. *Dependence on the Redshift Distribution of the Group Members*

Until now all group members were assumed to lie at the same redshift. For groups that have been selected from a spectroscopic survey with accurate redshift determinations, that will indeed be the case. However, it is instructive to investigate any qualitative differences that might arise in the shear profiles as a result of projection effects. Figure 9 shows the average shear around member galaxies for three cases in which (1) all member galaxies are at the same redshift, (2) half of the "member" galaxies are at a much higher redshift, and (3) the redshift difference is $\Delta z/z \sim 0.2$. As expected, a small redshift difference does not lead to significantly different results, whereas a larger redshift difference, with only part of the apparent group lying at an optimum lens redshift, leads to a decrease in the shear signal by a factor of a few. Note that the shape of the shear profiles is not affected by differences in redshift and that the measured ratio of the tangential shear at small radius to that at large radius is therefore still a good estimator of the relative halo : galaxy mass ratio. However, since the overall shear signal is reduced if galaxies are mistakenly assumed to be part of a group, the total mass in the group is likely to be systematically underestimated.

4.4. *Observational Uncertainties and Detection Feasibility in the Weak-Lensing Regime*

In the previous sections we have determined the expected weak-lensing signal of compact groups of galaxies and demonstrated that the average shear signal at a radial distance of 20″ from the galaxy centers varies by about 1% for different mass distributions in a sample of about 100 groups of galaxies. The questions arise, what data quality is necessary, and how many groups actually need to be observed in order to measure this difference significantly to discriminate between various mass models? There have been several recent attempts to measure the weak-lensing shear around galaxies on scales from 5″ to 60″. Wilson et al. (2001) measured the shear around about 5000 galaxies between redshifts of 0.1 and 0.9 in six 0.25 deg^2 fields observed with the Canada-France-Hawaii Telescope with an image quality of 0.″6 FWHM. After binning the galaxies into redshifts bins, they find a shear signal of 3%–4% with ±1% accuracy at 20″ distance for lens redshifts between 0.25 and 0.35 using 366 foreground and about 130,000 background galaxies with a median redshift of 1. Data of this quality is very nearly enough to distinguish the extreme cases for the mass distributions we have discussed above—with the same image quality, a sample of 800 galaxies contained in about 200 compact groups each with about 1000 background galaxies would provide tangential shear measurements at radii between 10″ and 20″ to better than 1% accuracy, making this distinction possible.

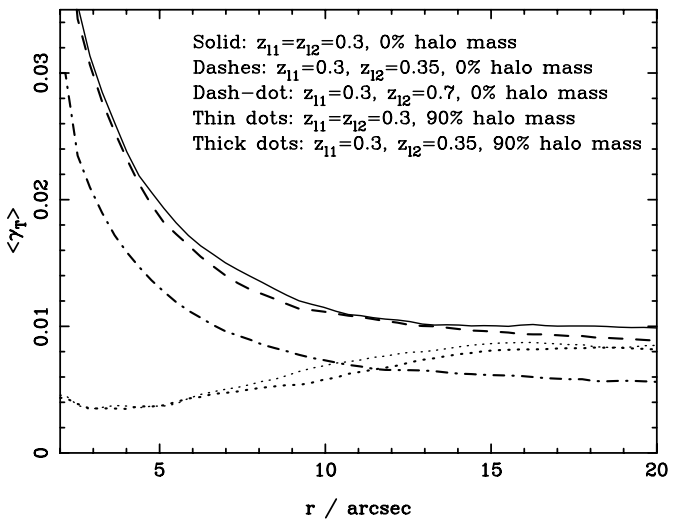

FIG. 9.—Average tangential shear around group members of 100 simulated groups for different lens redshifts. Results for projected groups in which the galaxies are at different redshifts are shown along with the results for compact groups at a single redshift of $z_l = 0.3$.

Below we outline the feasibility of the observational program suggested in the paper as a means of mapping the detailed mass distribution in galaxy groups. We estimate the number of groups that need to be stacked in order to distinguish between the various mass models. The dispersion in the shear σ_γ needed to distinguish models is of the order of 1% (this estimate reflects the difference in the averaged tangential shear between various models; see Fig. 6). Note that $\sigma_\gamma = \sigma_\epsilon/\sqrt{N}$, where $\sigma_\epsilon \sim 0.2$ is the width of the intrinsic ellipticity distribution and N is the total number of background galaxies whose shapes are sheared.

Since the shear is radially averaged in annuli around individual group members and the bulk of the signal is expected between 3″ and 8″ (range as seen in the x-axis of Fig. 6), the sampling needed (in units of number per arcmin^2) can be estimated as

$$n_0 = \left(\frac{\sigma_\epsilon}{\sigma_\gamma}\right)^2 \frac{1}{\pi(r_1^2 - r_0^2)} \sim 8300 \text{ arcmin}^{-2}\,, \qquad (18)$$

where $r_1 = 8''$ and $r_0 = 3''$ are the outer and inner annuli radii. For ground-based observations, galaxy number densities of 15–20 arcmin^{-2} are typical, yielding for a 2 σ detection (assuming a group with about four members) approximately 240 groups needing to be stacked. However, for space based observations, for instance with the proposed ACS on-board *HST*, the expected galaxy number density is about 60 arcmin^{-2}, implying that for a 3 σ detection of difference between mass models only 100 groups need to be stacked (see below for details), making it a very feasible and viable project.

We propose use of the ACS default pure parallel program to estimate the efficiency in detecting groups. In this mode, ACS will take one-half or one full orbit (∼1–2.5 ks exposures) in the F775W filter, and if they are available, complementary color images that could be used to determine the morphology of the group galaxies and the distance of the faint background galaxies, thus improving the statistics. In one orbit, it is expected to reach a limiting I-band magnitude of 26, for which we expect $(1–2) \times 10^5$ galaxies deg^{-2}, or 30–60 galaxies arcmin^{-2}. This translates into ∼100 groups (as quoted above) to get a 3 σ detection of the average

tangential shear at $\sim 5''$, which is sufficient to distinguish between the details of the various mass distributions. Extrapolating from the local abundance of groups $n_L = 1.4 \times 10^{-4}\ h^3\ \mathrm{Mpc}^{-3}$, we estimate that the area subtended by 100 groups on the sky is roughly 25 arcmin^2. However, to compute the total area that ACS needs to survey to detect 100 groups, we need to fold in the efficiency factor for detection, which is in fact the fraction of galaxies in groups. Using current estimates from ground-based redshift survey UZC-SSRS2 (Ramella et al. 2002), this factor is expected to be in the range of 0.35–0.43 (for compact groups with a membership of 5 or more at $z_l < 0.5$). Therefore, a total area of between 1 and 1.5 deg^2 needs to be surveyed by the ACS.

Observations in multiple bands would be helpful in order to obtain photometric redshifts for the background galaxies, thereby improving the accuracy. Since the selected groups are likely to be at redshifts of 0.4 or less, the expected uncertainty due to the unknown redshift distribution is expected to be small (see Bartelmann & Schneider 2001, Fig. 13), as the median redshift of the background galaxies will be about 1.

It is very difficult to predict systematic uncertainties for weak-lensing measurements, especially with new instruments, and there are still many systematic effects that are not perfectly understood. However, most of these effects have been shown to be small (Erben et al. 2001), and the success of past weak-lensing observations have shown that shear signals of order 1% can be reliably measured. With improved instruments (ACS) and larger data sets, it is expected that accuracy in shape measurements will improve to better than 0.5% on subarcminute scales.

5. STRONG-LENSING EFFECTS

In the previous section we calculated the expected magnitude of the weak-lensing signal due to galaxy groups. In this regime, there is clear observational evidence for the effect of the group potential. Many of the known lens systems cannot be described accurately by a single-lens model, and a significant external shear is required in many cases (Kundić et al. 1997a; Keeton, Kochanek, & Seljak 1997; Kneib, Cohen, & Hjorth 2000). In fact, groups of galaxies are found near many of these systems (Rusin et al. 2000). In general, the presence of a group in the vicinity of a galaxy lens will lead to an external shear contribution to the main lensing potential. The direction and magnitude of this shear will depend strongly on the precise mass distribution within the group, and this will affect the image positions, magnifications, time delays, and image geometries. This will be important both for modeling the individual lens systems as well as for determining the statistical properties of lens systems.

5.1. *Individual Lens Systems*

A basic consequence of the presence of a group on the lensing behavior of a nearby galaxy is to introduce some external shear. As shown for example by Keeton et al. (1997), the effect of this shear is to introduce an effective asymmetry in the potential that affects the image geometries and magnification ratios. In the following we investigate the effect of the details of the mass distribution inside the group that contains or neighbors closely, at the same redshift, an individual lensing galaxy.

5.1.1. *Magnification and Image Geometry*

Many of the expected properties of particular lens profiles can be determined from the "magnification map," which gives the total magnification as a function of source position on the source plane. The magnification map provides information on the number of images, the calculated magnifications, and the lensing cross sections (see Möller & Blain 1998). We compute the magnification map on the source plane for the simulated groups using ray tracing; the results for two models are shown in Figure 10. Comparison of the two panels in Figure 10 shows qualitatively how the properties of a group member depend on the relative masses of the galaxies within the group. The main differences and similarities in the magnification maps are the following:

1. The area inside the asteroid-shaped caustic is larger for the model with a more massive group halo owing to the convergence effect of κ. Sources that lie inside the asteroid-shaped caustics, seen in Figures 10*a* and 10*b*, are imaged into four magnified images. Therefore, in this particular configuration, the lensing galaxy is more likely to produce quadruple images if it is part of a group with a massive halo than if it is part of a group without such a halo.
2. The asteroid-shaped caustic line is longer for a more massive group halo. The probability that a small background source is magnified strongly is, to first order, proportional to the length of the caustic. Extended caustics are therefore more likely to produce high magnifications, and so, in this particular configuration, the lensing galaxy is more likely to produce strongly magnified images if it is part of a group with a massive halo.
3. The area inside the outer, circular caustic that surrounds the asteroid-shaped caustic, is independent of the mass distribution of the group. Sources that lie outside the area enclosed by this caustic are not multiply imaged, and, therefore, if observational magnification bias is ignored, the total strong-lensing cross section is not strongly dependent on the mass distribution of the group. One should not think that magnification bias is unlikely to be an issue here, as the increase in high magnification cross section due to the external shear is expected to be less than 10% for magnifications below 50.

From this we conclude that for individual lens systems that have neighboring groups, the details of the mass distribution in the group are expected to have a significant effect on the magnifications and image geometries.

5.1.2. *Lens Modeling and Time Delays*

Many strong gravitational lens systems have been used to estimate the Hubble parameter H_0 through a measurement of their time delay (e.g., Koopmans et al. 2000). Uncertainties in the derived value of H_0 are caused mainly by inaccuracies and uncertainties in models for the lensing potential. Many of these lens systems are part of, or lie near, a group (Kundić et al. 1997b), and it is therefore important to quantify the effect of the group on the measured time delay. Once again ray-tracing routines are used to compute the time delays for the various configurations.

Figure 11 shows the time delay as a function of image separation for the four different group mass distributions listed in Table 2. Despite the fact that the properties of the main galaxy are identical in all three panels, there is a significant variation in the time delay between different group models.

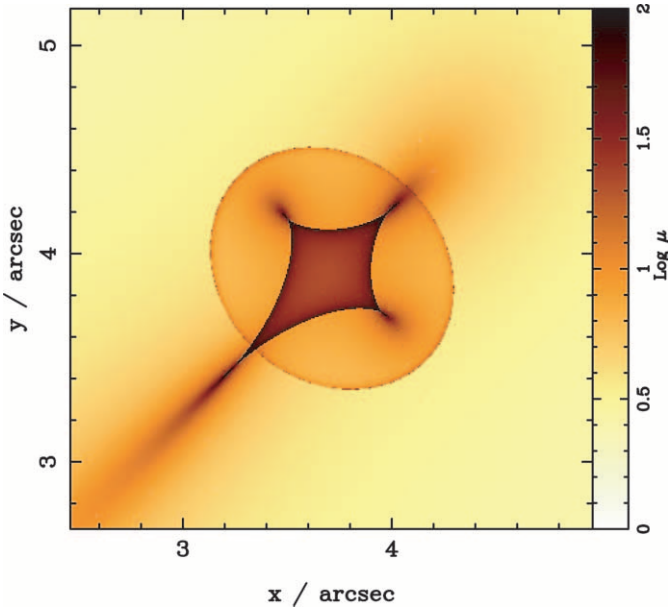

FIG. 10*a*

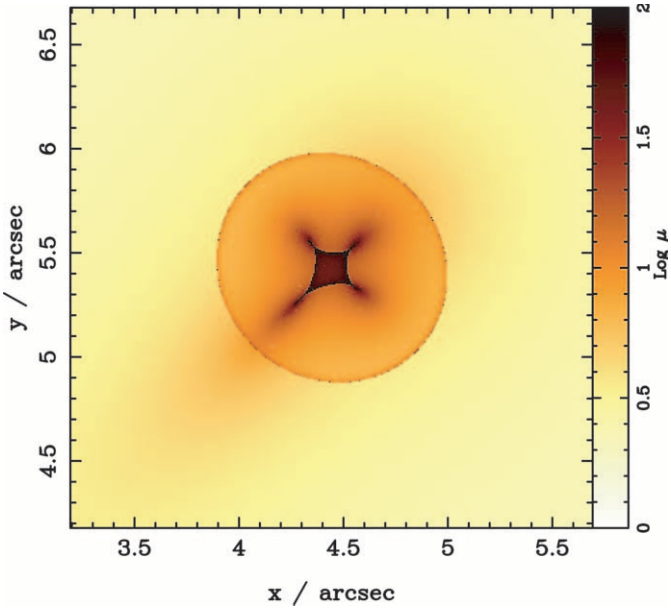

FIG. 10*b*

FIG. 10.—Magnification maps on the source plane for a typical compact group with four member galaxies. The panels are centered on the position of the main lensing galaxy, which has the same properties as galaxy 3 of model C (Table 2) in both panels. The properties of the group members vary: in (*a*), the group properties are those of model A; in (*b*), the group properties are those for model C. The diamond-shaped caustic along which magnifications are high is larger and more elongated in (*a*) than in (*b*). Note that the properties of the main lensing galaxy are the same in both panels and the differences in the maps arise solely from the variation of the mass distribution in the surrounding group.

The plot shows that the group potential itself has a great effect on the time delay; the presence of a massive group halo leads to smaller maximum image separations and larger time delays. Since $\Delta T \propto H_0^{-1}$, this has important consequences for the determination of H_0 from such systems. For example, for a lens system with image separations of $2''$, we estimate that the value of H_0 deduced from a time delay of about 80 days may vary from 100 km s^{-1} Mpc^{-1}, for a 70% halo, to 50 km s^{-1} Mpc^{-1} for no group halo. Therefore, depending on the relative mass of a group halo, the value of H_0 may be seriously underestimated if the group halo is not included in the lens modeling. Most recent lens models of systems near groups include an external shear contribution as a free parameter (e.g., Kundić 1997a) so that this effect is much smaller. However, modeling the surrounding group by a single external shear component, instead of taking the individual galaxies into account, might still lead to significant systematic errors in the determination of H_0. In the later stages of preparing this paper, Rusin et al. (2001) published a detailed analysis of the lens system B1359+154, demonstrating that the six-image configuration is in fact caused by a compact group of galaxies that acts as the lens. We will address general aspects of lens modeling of groups in detail in a future publication.

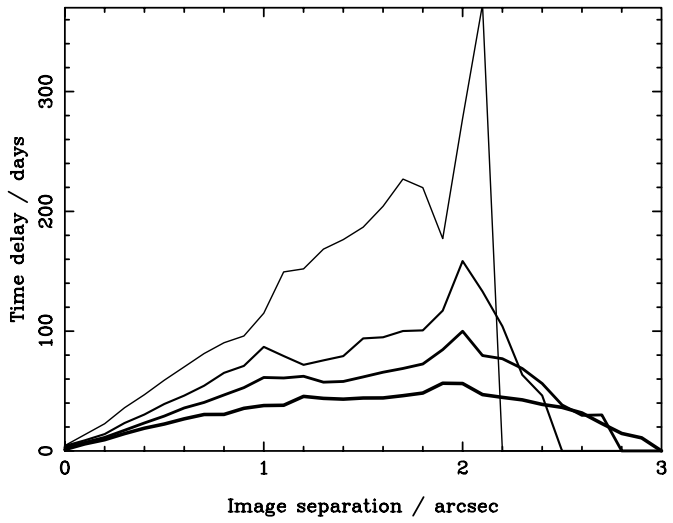

FIG. 11.—Time delay as a function of image separation for the different group models tabulated in Table 2. The curves are for models A, B, C, and D with increasing line thickness. As in Fig. 10, the main lensing galaxy has the same properties in all cases (galaxy 3, model C in Table 2).

5.2. *Statistical Strong Lensing*

In the following, we investigate the effect of the group mass distribution on strong-lensing statistics using the ray-tracing simulations and a sample of 100 random groups. By definition, each of these 100 groups contains one strong-lensing galaxy; the sample of 100 groups we refer to throughout this section is thus 100 groups *for which strong lensing is observed*. Such a sample does not yet exist; we discuss in § 5.3 when such a sample may be expected. In each group a single galaxy at position $\boldsymbol{r}_1$ is chosen to be the main lensing galaxy and we determine the magnifications, time delays, and image geometries for the lensing galaxy in each group, averaging the results for the whole sample. The groups are generated as described in § 2, except that we set the ellipticities of the individual galaxies $\epsilon = 0$ in the interest of computational speed. Our results will not be affected by the simplifying assumption that $\epsilon = 0$, since nonzero ellipticities introduce only an additional statistical error that is $\sim 0.2/\sqrt{N}$, where N is the number of lens systems in the sample.

TABLE 2
INDIVIDUAL GROUP MODELS

Parameter	Halo	Galaxy 1	Galaxy 2	Galaxy 3	Galaxy 4
x-position (arcsec)	0	30.0	−8.9	6.2	−17.3
y-position (arcsec)	0	−7.2	28.3	6.4	2.4
M in 100 kpc / 10^{11} $M_\odot$:					
Model A	155	2	6	8	1.2
Model B	120.7	6	18	23.9	3.6
Model C	86.2	10.1	30.1	40	6
Model D	0	20.2	60.1	80	12
Redshift z_l	0.3	0.3	0.3	0.3	0.3
r_s kpc^{-1}	15	0.3	0.5	0.7	0.1

NOTE.—Listed are the properties of the individual group models used in § 5 and Fig. 4.

For each system we obtain statistical information from the image information stored on a grid in the source plane, as described in § 3.1.2. In order to simulate observational selection effects, we also produce one set of results that only includes images with magnification ratios smaller than 20 and separations larger than 0.″1. We do not include magnification bias explicitly. This makes the results discussed below conservative, as magnification bias will increase the effect of groups on statistical lensing properties, since highly magnified sources are more probable in lens systems with substantial external shear.

5.2.1. *Multiplicity of Images, Image Separations, and Magnification Ratios*

We determined the image separations and magnification ratios for all image pairs for all 100 groups in the simulated sample. Investigating the statistics of the number of images, we found that changing the mass distribution inside the group had little effect; the cross sections for lensing into three, four, and five images varied by less than 10%. This shows that even though image multiplicities of individual systems may be influenced strongly by the particular direction and magnitude of the shear, the average effect for a large sample of lens systems is small.

The maximum image separations depend on the projected mass contained inside the smallest circle that contains all images (Schneider et al. 1992). Therefore, external shear that involves only a contribution to γ will not affect the maximum image separations unless the image multiplicities are increased. The presence of a group will affect the maximum image separations only if there is a significant contribution to the mean κ from the group.

Figure 12 shows the distribution of image separations for different group mass distributions for four different choices of the relative position between lensing galaxy and group. The distance of the lensing galaxy from the group center is determined randomly from the distribution given by equation (4). The figure shows that, as expected, massive group halos lead to slightly larger separations. This effect is in principle detectable, given a sample of 100 appropriate lens systems. However, in practice some additional information is needed to disentangle the degeneracy between a contribution to κ due to a separate group halo component and due to a more massive individual lens galaxy. Figure 12 also shows the significant effect of selection criteria on lensing statistics. If useful information about the lens population is to be gained from lens statistics, the observational selection criteria need to be better understood.

The magnification ratio $\mu_r = \mu_A/\mu_B$ for two images A and B is given by equation (12). In the case $\kappa_A \approx \kappa_B \approx 0$, the magnification ratio can be approximated as $\mu_r = (1 - \gamma_B^2)/(1 - \gamma_A^2)$. If γ varies significantly over distances of the order of the image separations ($\approx 1''$), then the magnification ratios are expected to be larger than if γ varies only slightly. Thus, any variation of the external shear due to differences of the mass distribution of the group may change the distribution of magnification ratios.

Figure 13 shows the distribution of magnification ratios for different group mass distributions. The figure shows that massive group halos lead to slightly larger magnification ratios, but the effect is small (<15%). As in Figure 12, observational selection effects change the statistics significantly, even for relatively low magnification ratios of $\mu_r \approx 5$.

5.2.2. *Effect on the Time Delay*

Now we assess the effect of the detailed mass distribution on the statistical time delay of a larger sample of lens systems (note that the time delay was determined as described in § 3.1.2).

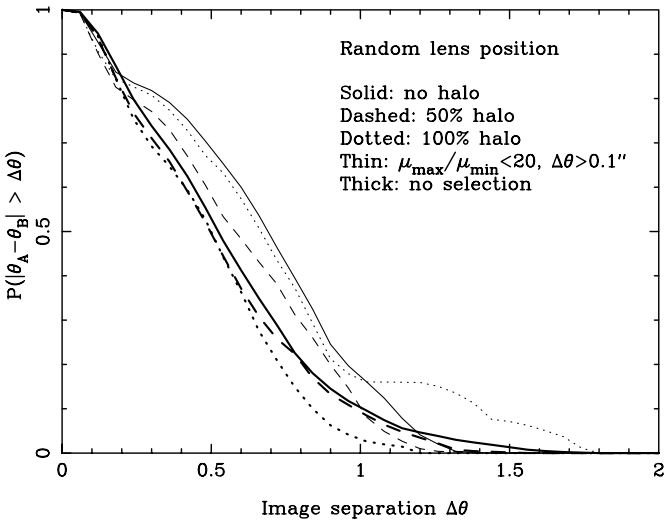

FIG. 12.—Distribution of image separations expected for a large sample of strong lens systems. The curves are obtained by binning the angular separation $\Delta\theta = |\boldsymbol{\theta}_A - \boldsymbol{\theta}_B|$ for each pair of images of a given source. Each lensing galaxy is at a random position within the group, determined using eq. (4). The statistics shown in the thin curves include only images that are separated by more than 0.″1 and have a magnification ratio less than 1 : 20.

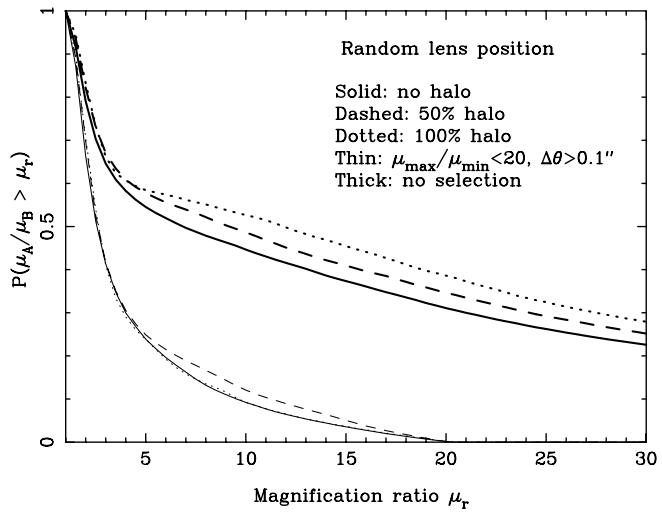

FIG. 13.—Magnification ratio distribution expected for a large sample of strong lens systems. The curves are obtained by binning the magnification ratio for each pair of images of a given source. The positioning of the lens galaxy is random and the line styles are as in Fig. 12.

For each source, the maximum time delay between image pairs is binned to create the curves shown in Figure 14. Figures 14*a*–14*c* show the results for separations $\delta\phi = |\boldsymbol{r}_h - \boldsymbol{r}_l|$ between the lensing galaxy and the group center at $\boldsymbol{r}_h$ of $\delta\phi = 5''$, $\delta\phi = 10''$ and $\delta\phi = 30''$, respectively. In Figure 14*d* the distance of the lensing galaxy from the group center is determined randomly from the distribution given by equation (4). Strong lens systems in which the main lensing galaxy is associated with a group that contains a massive group halo are more likely to have larger time delays if the main lensing galaxy is located close to the group center. Lens systems in groups without a massive large-scale halo will have more strongly peaked time-delay distributions with a maximum around the corresponding average Einstein radius. In the case that the lensing galaxy is farther away from the group center, the halo has a smaller effect and the time delays are on average smaller for groups with a large halo : galaxy mass fraction, due to the smaller mass contained in the individual galaxies. Since the galaxies are, on average, farther away than 10″, systems with massive group halos are on average 30% less likely to produce time delays of 10 days or more. Thus, measuring the time delays of a sample of about 100 lens systems associated with compact groups

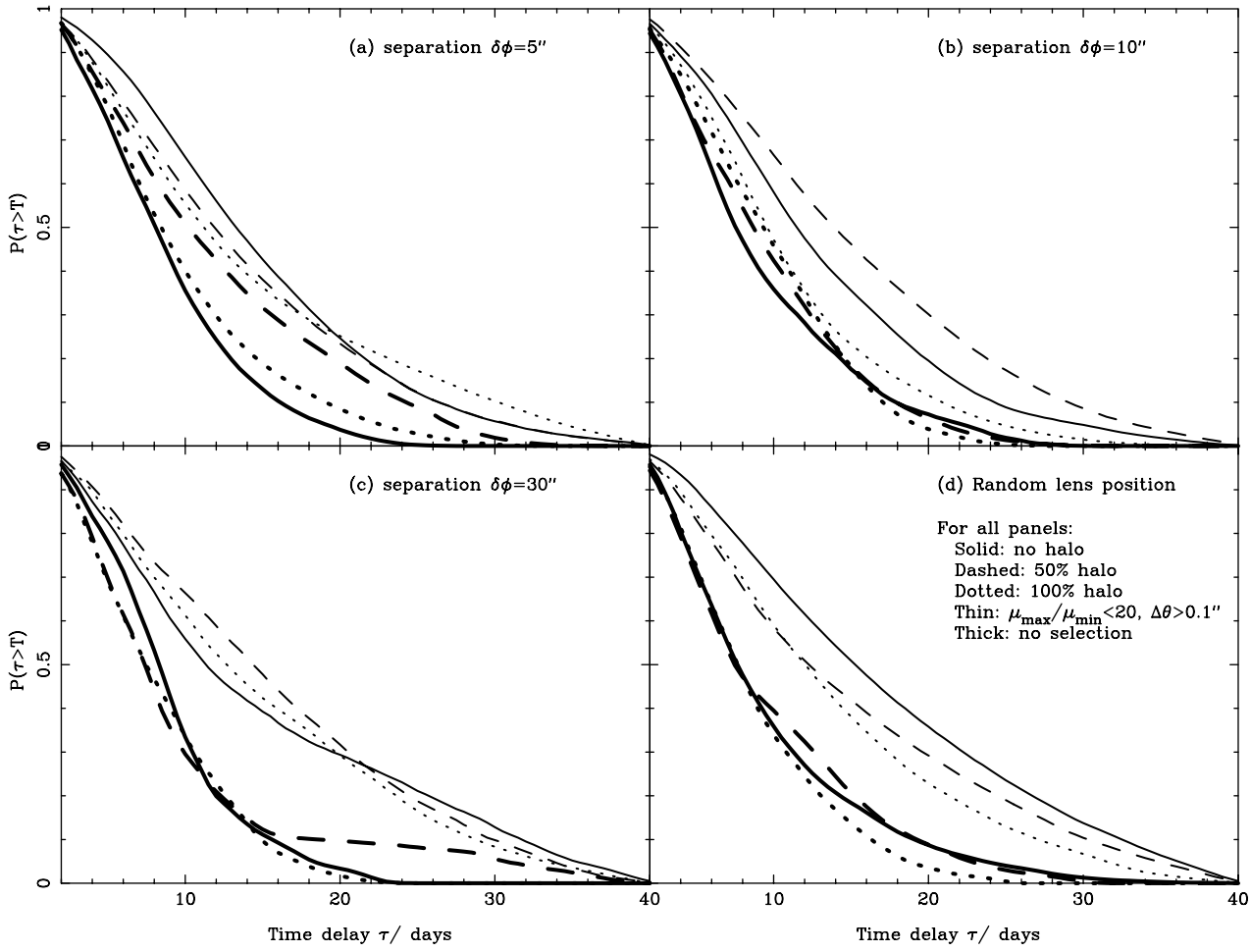

FIG. 14.—Time-delay statistics for different halo masses, from simulations of 100 group systems. The curves show the fraction of systems with a time delay τ larger than T that are expected in a large sample of strong lens systems which are associated with compact groups; (*a–c*) show the results for three different separations between the lensing galaxy and the group center, $\delta\phi$. In (*d*) the distance of the lensing galaxy from the group center is determined randomly from the distribution given by eq. (4).

could provide information on the mass distribution in groups, provided the value of H_0 is known. If the value of H_0 is to be deduced from a statistical sample of lens galaxies, care has to be taken to account fully for the presence of groups. If a significant number of individual lens systems used to determine H_0 are near groups with massive halos, not taking the group into account may not only give a very bad fit to the multiple images (especially for quadruple images), but might also lead to a systematic significant underestimate of the value of H_0.

5.3. *Observational Possibilities in the Strong-Lensing Regime*

Whether strong lensing can be used to determine the mass distribution in groups will depend mainly on the lens sample. If the mass distribution inside a particular strong-lensing group is to be obtained, detailed modeling of the group potential requires a lens system with many constraints—a four-image system with measured image positions and magnification ratios is unlikely to be sufficient. Some systems of lensed extended radio sources have been found (Myers et al. 1999; Rusin et al. 2000). In those systems, the individual source components provide a number of additional constraints, and it is those systems for which detailed mass modeling of the group is most likely to succeed. Unfortunately, only very few of these lens systems have been discovered so far. In order to constrain the mass distribution in groups from statistics of strong lensing, as described in § 5.2, a large number of lens systems that are part of or near to a group are required. Presently, the number of known lens systems is too small. Keeton et al. (2001) estimate that a fraction of at least 20% lens galaxies reside in groups. From our results in § 5.2.2, one estimates that about 200 time delays above 10 days need to be measured to be able to determine the time delay distribution with better than 10% accuracy, which would be needed to distinguish between the mass distributions, as shown in Figure 14*d*. If time delays can be measured for only about 50% of the lens systems, we conclude that a sample of at least 2000 lens galaxies are required, roughly 40 times the number of lens systems known to date. This is a large number, but future instruments and surveys are likely to increase the number of known lens systems by at least an order of magnitude. The *Planck Surveyor* satellite will find about 1000 lens systems serendipitously (Blain 1998) and the Atacama Large Millimeter Array (ALMA) will make it possible to follow up all these lens systems and measure image positions, magnification ratios, and time delays very accurately.

For the moment, however, constraints on the mass distribution of galaxy groups from strong lensing are most likely achieved by detailed modeling of individual lens systems (Rusin et al. 2001).

6. CONCLUSIONS

Even though velocity dispersions can be measured to constrain the total mass of groups (Mahdavi et al. 2000), the mass distribution inside groups is currently not well known. If additional assumptions about the correlation between X-ray luminosity and mass density are made, details of the dark matter distribution can be obtained from sensitive, high-resolution X-ray images. Only gravitational lensing provides a direct probe of the surface mass density and its spatial distribution. In this paper, we demonstrate using numerical techniques that weak and strong gravitational lensing can be used to constrain both the total mass as well as the details of the mass distribution in groups.

In summary, the results for weak-lensing properties groups are as follows:

1. The weak-lensing shear signal of groups at $r \sim 10''$ is about 3%, and it varies by up to a factor of 2 for different mass distributions. More importantly, the ratio of the tangential shear at small radii to that at larger distances varies by a factor of a few depending on the mass contained in the group halo.
2. This effect is not detectable for an individual group, but if about 100 groups are stacked (using the ACS for instance), then the shear signal around the individual member galaxies can be determined with sufficient accuracy to distinguish different mass profiles. The stacking of a large number of groups also decreases the noise due to cosmic variance, which is of the same magnitude as the shear signal for individual groups, to a level of about 1% of the total group signal.
3. Averaging the shear signal around individual group members has many practical advantages; the measured shear at larger radii provides information on the total group mass, whereas the average shear close to the galaxies measures the galaxy mass fraction.
4. The qualitative results (features in the radially averaged tangential shear profile) are independent of the form of the number density profile assumed, the halo scale length, and possible projection effects. The level of the signal depends on the details of the density profile, halo scale length, and redshifts; however, the form of the shear profile as a function of radius remains the same and is determined only by the halo mass fraction.
5. With new instruments, such as ACS on *HST*, it should be possible to determine the shear to a sufficient accuracy, to distinguish different group mass distributions. In particular, it should be viable to determine whether groups possess a significant large-scale dark halo or not.

The prospect of combining lensing data with X-ray data to probe the mass distribution in galaxy groups is promising, especially in the light of current high-resolution imaging X-ray satellites (Markevitch et al. 1999; Ettori & Fabian 2000).

The synopsis of our strong-lensing results is the following:

1. In the strong-lensing regime the presence of groups and the mass distribution within the group can affect the magnification maps and caustic structure significantly for an individual lens in the vicinity. The observed time delay is particularly sensitive to the details of the mass distribution in the surrounding group. This systematic error needs to be taken into account carefully when making estimates of H_0 from time-delay measurements.
2. In individual lens systems, the probability of multiple imaging into three or more images may be increased in cases where the main lensing galaxy is part of or very close to a group. In particular, lens models which do not take the presence of the group into account are likely to underestimate the cross section for high image multiplicities.
3. Statistically, the magnification ratios of images with large separations are larger for lensing galaxies that are part of groups with a massive halo.

4. The statistics of time delays can also be used to constrain the mass distribution in groups; lens systems in groups with a high halo mass fraction are 30% less likely to produce time delays of 10 days or more.

5. Detailed modeling of lens systems with multiple image components are likely provide constraints on the mass distribution of groups. Planck and ALMA will find 1000 or more lens systems, enough to use lens statistics to constrain the mass distribution in groups.

Weak and strong gravitational lensing studies can provide important constraints on the mass content and distribution of mass in groups of galaxies.

The authors acknowledge the Lensnet TMR network for support. J. P. K. acknowledges support from the CNRS. A. W. B. acknowledges financial support from the Raymond and Beverly Sackler foundation as part of the Foundation's Deep Sky Initiative programme at the IoA. We thank the referee for thoughtful and extremely useful comments that have substantially improved our paper.

REFERENCES

Bartelmann, M., Huss, A., Colberg, J. M., Jenkins, A., & Pearce, F. R. 1998, A&A, 330, 1
Bartelmann, M., & Schneider, P. 2001, Phys. Rep., 340, 291
Barton, E., Geller, M., Ramella, M., Marzke, R. O., & da Costa, L. N. 1996, AJ, 112, 871
Blain, A. W. 1998, MNRAS, 297, 511
Brainerd, T. G., Blandford, R. D., & Smail, I. R. 1996, ApJ, 466, 623
Clowe, D., Luppino, G. A., Kaiser, N., & Gioia, I. M. 2000, ApJ, 539, 540
Cohn, J. D., Kochanek, C. S., McLeod, B. A., & Keeton, C. R. 2001, ApJ, 554, 1216
de Carvalho, R. R., & Djorgovski, S. G. 1995, BAAS, 187, 53.02
dell'Antonio, I. P., & Tyson, J. A. 1996, ApJ, 473, L17
Erben, T., van Waerbeke, L., Bertin, E., Mellier, Y., & Schneider, P. 2001, A&A, 366, 717
Ettori, S., & Fabian, A. C. 2000, MNRAS, 317, L57
Fischer, P. 1999, AJ, 117, 2024
———. 2000, AJ, 120, 1198
Geiger, B., & Schneider, P. 1999, MNRAS, 302, 118
Girardi, M., & Giuricin, G. 2000, ApJ, 540, 45
Helsdon, S. F., & Ponman, T. J. 2000, MNRAS, 315, 356
Helsdon, S. F., Ponman, T. J., O'Sullivan, E., & Forbes, D. A. 2001, MNRAS, 325, 693
Hickson, P. 1982, ApJ, 255, 382
Hickson, P., Kindl, E., & Huchra, J. P. 1988, ApJ, 329, L65
Hickson, P., Mendes de Oliviera, C., Huchra, J. P., & Palumbo, G. G. 1992, ApJ, 399, 353
Hoekstra, H., et al. 2001, ApJ, 548, L5
Hoekstra, H., Franx, M., & Kuijken, K. 2000, ApJ, 532, 88
Hoekstra, H., Franx, M., Kuijken, K., & Squires, G. 1998, ApJ, 504, 636
Hudson, M. J., Gwyn, S. D. J., Dahle, H. & Kaiser, N. 1998, ApJ, 503, 531
Kaiser, N. 1995, ApJ, 439, L1
Kassiola, A., & Kovner, I. 1993, ApJ, 417, 450
Keeton, C. R., Christlen, D., & Zabludoff, A. I. 2000, ApJ, 545, 129
Keeton, C. R., Kochanek, C. S., & Seljak, U. 1997, ApJ, 482, 604
Kneib, J., Cohen, J. G., & Hjorth, J. 2000, ApJ, 544, L35
Koopmans, L. V. E., de Bruyn, A. G., Xanthopoulos, E., & Fassnacht, C. D. 2000, A&A, 356, 391
Kundić, T., Hogg, D. W., Blandford, R. D., Cohen, J. G., Lubin, L. M., & Larkin, J. E. 1997a, AJ, 114, 2276
Kundić, T., et al. 1997b, ApJ, 482, 75
Mahdavi, A., Böhringer, H., Geller, M. J., & Ramella, M. 2000, ApJ, 534, 114
Markevitch, M., Vikhlinin, A., Forman, W. R., & Sarazin, C. L. 1999, ApJ, 527, 545
McKay, T. A., et al. 2001, ApJ, submitted (astro-ph/0108013)
Mellier, Y. 1999, ARA&A, 37, 127
Möller, O., & Blain, A. W. 1998, MNRAS, 299, 845
———. 2001, MNRAS, 327, 339
Mulchaey, J. S., & Zabludoff, A. I. 1998, ApJ, 496, 73
Myers, S. T., et al. 1999, AJ, 117, 2565
Natarajan, P., & Kneib, J. 1997, MNRAS, 287, 833
Natarajan, P., Kneib, J., Smail, I., & Ellis, R. S. 1998, ApJ, 499, 600
Navarro, J., Frenk, C. S., & White, S. D. M. 1996, ApJ, 462, 563
Ponman, T. J., et al. 1995, Nature, 369, 462
Press, W. H., & Schechter, P. 1974, ApJ, 187, 425
Press, W. H., et al. 1988, Numerical Recipes (Cambridge: Cambridge Univ. Press)
Ramella, M., Geller, M. J., Pisani, A., & da Costa, L. N. 2002, preprint (astro-ph/0202326)
Ramella, M., Pisani, A., & Geller, M. J. 1997, AJ, 113, 483
Ramella, M., et al. 1999, A&A, 342, 1
Rusin, D., Hall, P. B., Nichol, R. C., Marlow, D. R., Richards, A. M. S., & Myers, S. T. 2000, ApJ, 533, L89
Rusin, D., et al. 2001, ApJ, 557, 594
Schneider, P., Ehlers, J., & Falco, E. E. 1992, Gravitational Lenses (Berlin: Springer)
Schneider, P., van Waerbeke, L., Jain, B., & Kruse, G. 1998, MNRAS, 296, 873
Schramm, T. 1990, A&A, 231, 19
Trentham, N., Möller, O., & Ramirez-Ruiz, E. 2001, MNRAS, 322, 658
Wambsganss, J., Cen, R., & Ostriker, J. P. 1998, ApJ, 494, 29
Wilson, G., Kaiser, N., Luppino, G. A., & Cowie, L. L. 2001, ApJ, 555, 572
Wright, C. O., & Brainerd, T. G. 2000, ApJ, 534, 34
Zabludoff, A., & Mulchaey, J. 1998, ApJ, 496, 39
———. 2000, ApJ, 539, 136